The Astrophysical Journal, 700:137–148, 2009 July 20 doi:10.1088/0004-637X/700/1/137

TRIGONOMETRIC PARALLAXES OF MASSIVE STAR-FORMING REGIONS. VI. GALACTIC STRUCTURE, FUNDAMENTAL PARAMETERS, AND NONCIRCULAR MOTIONS

M. J. Reid[1], K. M. Menten[2], X. W. Zheng[3], A. Brunthaler[2], L. Moscadelli[4], Y. Xu[2,5], B. Zhang[3], M. Sato[1,6], M. Honma[6], T. Hirota[6], K. Hachisuka[7], Y. K. Choi[2], G. A. Moellenbrock[8], and A. Bartkiewicz[9]

[1] Harvard-Smithsonian Center for Astrophysics, 60 Garden Street, Cambridge, MA 02138, USA
[2] Max-Planck-Institut für Radioastronomie, Auf dem Hügel 69, 53121 Bonn, Germany
[3] Department of Astronomy, Nanjing University Nanjing 210093, China
[4] Arcetri Observatory, Firenze, Italy
[5] Purple Mountain Observatory, Chinese Academy of Sciences, Nanjing 210008, China
[6] VERA Project, National Astronomical Observatory, Tokyo 181 8588, Japan
[7] Shanghai Astronomical Observatory, 80 Nandan Road, Shanghai, China
[8] National Radio Astronomy Observatory, Socorro, NM, USA
[9] Torun Centre for Astronomy, Nicolaus Copernicus University, Gagarina 11, 87-100 Torun, Poland
Received 2009 February 16; accepted 2009 May 14; published 2009 June 30

ABSTRACT

We are using the Very Long Baseline Array and the Japanese VLBI Exploration of Radio Astronomy project to measure trigonometric parallaxes and proper motions of masers found in high-mass star-forming regions across the Milky Way. Early results from 18 sources locate several spiral arms. The Perseus spiral arm has a pitch angle of $16^\circ \pm 3^\circ$, which favors four rather than two spiral arms for the Galaxy. Combining positions, distances, proper motions, and radial velocities yields complete three-dimensional kinematic information. We find that star-forming regions on average are orbiting the Galaxy ≈15 km s^{-1} slower than expected for circular orbits. By fitting the measurements to a model of the Galaxy, we estimate the distance to the Galactic center $R_0 = 8.4 \pm 0.6$ kpc and a circular rotation speed $\Theta_0 = 254 \pm 16$ km s^{-1}. The ratio Θ_0/R_0 can be determined to higher accuracy than either parameter individually, and we find it to be 30.3 ± 0.9 km s^{-1} kpc^{-1}, in good agreement with the angular rotation rate determined from the proper motion of Sgr A*. The data favor a rotation curve for the Galaxy that is nearly flat or slightly rising with Galactocentric distance. Kinematic distances are generally too large, sometimes by factors greater than 2; they can be brought into better agreement with the trigonometric parallaxes by increasing Θ_0/R_0 from the IAU recommended value of 25.9 km s^{-1} kpc^{-1} to a value near 30 km s^{-1} kpc^{-1}. We offer a "revised" prescription for calculating kinematic distances and their uncertainties, as well as a new approach for defining Galactic coordinates. Finally, our estimates of Θ_0 and Θ_0/R_0, when coupled with direct estimates of R_0, provide evidence that the rotation curve of the Milky Way is similar to that of the Andromeda galaxy, suggesting that the dark matter halos of these two dominant Local Group galaxy are comparably massive.

Key words: astrometry – Galaxy: fundamental parameters – Galaxy: halo – Galaxy: kinematics and dynamics – Galaxy: structure – stars: formation

Online-only material: color figures, tar files

1. INTRODUCTION

The Milky Way is known to possess spiral structure. However, revealing the nature of this structure has proven to be elusive for decades. The Georgelin & Georgelin (1976) study of H II regions produced what has been generally considered the "standard model" for the spiral structure of the Galaxy. However, after decades of study there is little agreement on this structure. Indeed, we do not really know the number of spiral arms (Simonson 1976; Cohen et al. 1980; Bash 1981; Vallée 1995; Drimmel 2000; Russeil 2003) or how tightly wound is their pattern. The primary reason for the difficulty is the lack of accurate distance measurements throughout the Galaxy. Photometric distances are prone to calibration problems, which become especially severe when looking through copious dust to distant objects in the plane of the Galaxy. Thus, most attempts to map the Galaxy rely on radio frequency observations and kinematic distances, which involve matching source Doppler shifts with those expected from a model of Galactic rotation. However, because of distance ambiguities in the first and fourth quadrants (where most of the spiral arms are found) and the existence of sizeable noncircular motions, kinematic distances can be highly uncertain (Burton & Bania 1974; Liszt & Burton 1981; Gómez 2006).

We are measuring trigonometric parallaxes and proper motions of sources of maser emission associated with high-mass star-forming regions (HMSFRs), using the National Radio Astronomy Observatory's[10] Very Long Baseline Array (VLBA) and the Japanese VLBI Exploration of Radio Astronomy (VERA) project. The great advantage of trigonometric parallaxes and proper motions is that one determines source distances directly and geometrically, with no assumptions about luminosity, extinction, metallicity, crowding, etc. Also, from the same measurements, one determines proper motions, and if the time sampling is optimal there is little if any correlation between the parallax and proper motion estimates. Thus, the magnitude of the proper motion does not affect the parallax accuracy. Combining all of the observational data yields the full three-dimensional locations and velocity vectors of the sources.

Results for 12 GHz methanol (CH_3OH) masers toward 10 HMSFRs, carried out with the VLBA (program BR100), are

[10] The National Radio Astronomy Observatory is a facility of the National Science Foundation operated under cooperative agreement by Associated Universities, Inc.

Table 1
Parallaxes and Proper Motions of High-mass Star-Forming Regions

Source	ℓ (deg)	b (deg)	Parallax (mas)	μ_x (mas yr^{-1})	μ_y (mas yr^{-1})	$v_{\rm LSR}$ (km s^{-1})	Ref.
G 23.0−0.4	23.01	−0.41	0.218 ± 0.017	−1.72 ± 0.04	−4.12 ± 0.30	+81 ± 3	V
G 23.4−0.2	23.44	−0.18	0.170 ± 0.032	−1.93 ± 0.10	−4.11 ± 0.07	+97 ± 3	V
G 23.6−0.1	23.66	−0.13	0.313 ± 0.039	−1.32 ± 0.02	−2.96 ± 0.03	+83 ± 3	1
G 35.2−0.7	35.20	−0.74	0.456 ± 0.045	−0.18 ± 0.06	−3.63 ± 0.11	+28 ± 3	IV
G 35.2−1.7	35.20	−1.74	0.306 ± 0.045	−0.71 ± 0.05	−3.61 ± 0.17	+42 ± 3	IV
W 51 IRS 2	49.49	−0.37	0.195 ± 0.071	−2.49 ± 0.08	−5.51 ± 0.11	+56 ± 3	III
G 59.7+0.1	59.78	+0.06	0.463 ± 0.020	−1.65 ± 0.03	−5.12 ± 0.08	+27 ± 3	III
Cep A	109.87	+2.11	1.430 ± 0.080	+0.50 ± 1.10	−3.70 ± 0.20	−10 ± 5	II
NGC 7538	111.54	+0.78	0.378 ± 0.017	−2.45 ± 0.03	−2.44 ± 0.06	−57 ± 3	II
IRAS 00420	122.02	−7.07	0.470 ± 0.020	−1.99 ± 0.07	−1.62 ± 0.05	−44 ± 5	2
NGC 281	123.07	−6.31	0.355 ± 0.030	−2.63 ± 0.05	−1.86 ± 0.08	−31 ± 5	3
W3(OH)	133.95	+1.06	0.512 ± 0.010	−1.20 ± 0.20	−0.15 ± 0.20	−45 ± 3	4
WB 89-437	135.28	+2.80	0.167 ± 0.006	−1.27 ± 0.50	+0.82 ± 0.05	−72 ± 3	5
S 252	188.95	+0.89	0.476 ± 0.006	+0.02 ± 0.01	−2.02 ± 0.04	+11 ± 3	I
S 269	196.45	−1.68	0.189 ± 0.016	−0.42 ± 0.02	−0.12 ± 0.08	+20 ± 3	6
Orion	209.01	−19.38	2.425 ± 0.035	+3.30 ± 1.00	+0.10 ± 1.00	+10 ± 5	7
G 232.6+1.0	232.62	+1.00	0.596 ± 0.035	−2.17 ± 0.06	+2.09 ± 0.46	+23 ± 3	I
VY CMa	239.35	−5.06	0.876 ± 0.076	−3.24 ± 0.16	+2.06 ± 0.60	+18 ± 3	8

Notes. Columns 2 and 3 give Galactic longitude and latitude, respectively. Columns 5 and 6 are proper motions in the eastward ($\mu_x = \mu_\alpha \cos\delta$) and northward directions ($\mu_y = \mu_\delta$), respectively. Column 7 lists local standard of rest (LSR) velocity components; these can be converted to a heliocentric frame as described in the Appendix.

References. References are (I) Reid et al. 2009; (II) Moscadelli et al. 2009; (III) Xu et al. 2009; (IV) Zhang et al. 2009; (V) Brunthaler et al. 2009; (1) Bartkiewicz et al. 2008; (2) Moellenbrock et al. 2007; (3) Sato et al. 2008; (4) Xu et al. 2006; Hachisuka et al. 2006; (5) Hachisuka et al. 2009; (6) Honma et al. 2007; (7) Hirota et al. 2007; Menten et al. 2007; (8) Choi et al. 2008. The calculations in this paper use an early parallax and proper motion estimate for IRAS 00420+5530 cited above; the values reported more recently by Moellenbrock et al. (2009) are slightly different but would not substantively change the results presented here.

reported in the first five papers in this series (Reid et al. 2009; Moscadelli et al. 2009; Xu et al. 2009; Zhang et al. 2009; Brunthaler et al. 2009), hereafter Papers I through V, respectively. Eight other sources with H_2O or SiO masers have been measured with VERA (Honma et al. 2007; Hirota et al. 2007; Choi et al. 2008; Sato et al. 2008) and with methanol, H_2O or continuum emission with the VLBA (Hachisuka et al. 2006; Menten et al. 2007; Moellenbrock et al. 2007; Bartkiewicz et al. 2008; Hachisuka et al. 2009). In this paper, we collect these parallaxes and proper motions in order to study the spiral structure of the Galaxy. Combining positions, distances, Doppler shifts, and proper motions, allows us not only to locate the HMSFRs that harbor the target maser sources in three dimensions, but also to determine their three-dimensional space motions. In Section 2, we map the locations of the HMSFRs and measure the pitch angles of some spiral arms. In Section 3, we use the full three-dimensional spatial and kinematic information to examine the noncircular (peculiar) motions of these star-forming regions. We also fit the data with a model of the Galaxy and estimate the distance from the Sun to the Galactic center (R_0) and the circular orbital speed at the Sun (Θ_0). The nature of the rotation curve and its effect on estimates of R_0 and Θ_0 is also discussed. In Section 4, we compare kinematic distances with those determined by trigonometric parallax and offer a new prescription to improve such distance estimates. In Section 5, we discuss limitations of the current definition of Galactic coordinates and suggest a new system based partly on dynamical information. Finally, we discuss the broader implications of our results in Section 6.

2. GALACTIC SPIRAL STRUCTURE

Table 1 summarizes the parallax and proper motions of 18 regions of high-mass star formation measured with very long baseline interferometry (VLBI) techniques. The locations of these star-forming regions in the Galaxy are shown in Figure 1, superposed on an artist's conception of the Milky Way. Distance errors are indicated with error bars (1σ), but for most sources the error bars are smaller than the dots.

2.1. Spiral Arms

The HMSFRs with parallaxes locate several spiral arms. The three sources closest to the Galactic center (G 23.0−0.4, G 23.4−0.2, and G 23.6−0.1) appear to be members of the Crux–Scutum or possibly the Norma or the 3 kpc arm. However, the parallax uncertainties for these distant, low-declination sources are currently not adequate to clearly distinguish among these arms, especially in the crowded region where the Galactic bar (see Blitz & Spergel (1991b), and references therein) ends and the arms begin (Benjamin et al. 2005; Dame & Thaddeus 2008).

Three sources (G 35.2−0.7, G 35.2−1.7, and W 51 IRS 2) are probably in the Carina–Sagittarius arm, whose distance from the Sun is 2.5 kpc at Galactic longitude, ℓ, of $\approx 35^\circ$.

Five sources (S 252, W3(OH), IRAS 00420+5530, NGC 281, and NGC 7538) clearly trace a portion of the Perseus arm, which is located between distances of 2.10 kpc at $\ell = 189^\circ$ (S 252) and 2.64 kpc at $\ell = 112^\circ$ (NGC 7538). NGC 281 is slightly offset from the other sources in the Perseus arm and is believed to be associated with an expanding super-bubble (Sato et al. 2008). As such, it may not accurately trace spiral structure.

Two sources, (S 269 and WB 89-437), measured by Honma et al. (2007) with the VERA array and Hachisuka et al. (2009) with the VLBA, lie beyond the Perseus arm and begin to trace an Outer (Cygnus) arm at a distance from the Sun of 5.3 kpc at $\ell = 196^\circ$ for S 269 to 5.9 kpc at $\ell = 135^\circ$ for WB 89-437.

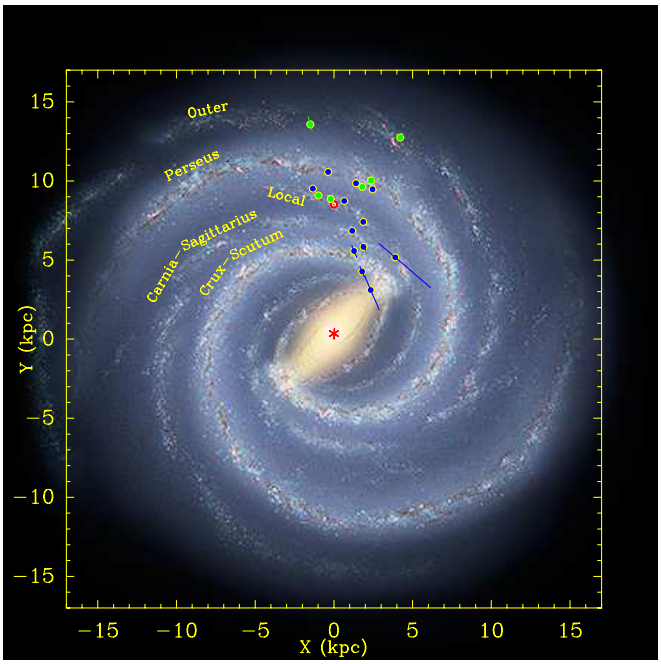

Figure 1. Locations of HMSFRs for which trigonometric parallaxes have been measured. Parallaxes from 12 GHz methanol masers are indicated with dark blue dots and those from H_2O and SiO masers or continuum emission (Orion) are indicated with light green dots. Distance error bars are indicated, but most are smaller than the dots. The Galactic center (red asterisk) is at (0, 0) and the Sun (red Sun symbol) at (0, 8.5). The background is an artist's conception of Milky Way (R. Hurt: NASA/JPL-Caltech/SSC) viewed from the north Galactic pole from which the Galaxy rotates clockwise. The artist's image has been scaled to place the HMSFRs in the spiral arms, some of which are labeled.

(A color version of this figure is available in the online journal.)

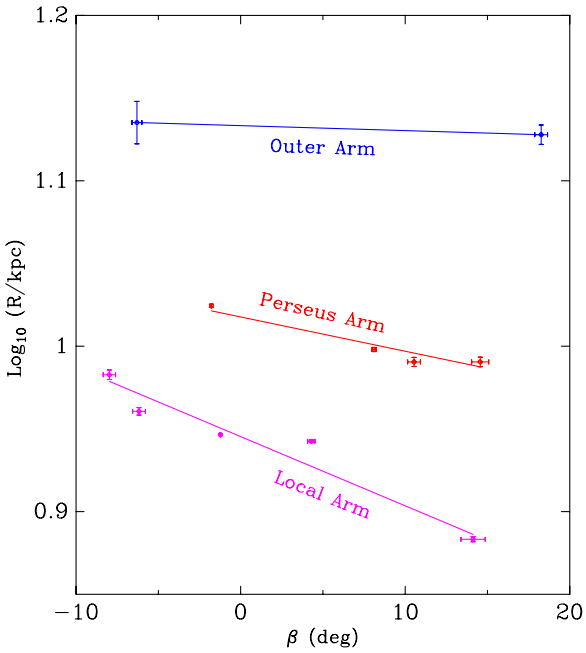

Figure 2. Spiral arm pitch angles. The logarithm of Galactocentric radius, R, (in kpc units) is plotted against Galactocentric longitude (β). Data based on trigonometric parallaxes for sources that can be confidently assigned to a spiral arm are shown along with 1σ uncertainties. Positional variations of star forming regions within an arm are clearly greater than the parallax uncertainties. Unweighted fits of straight lines to the data are shown with solid lines. Pitch angles are proportional to the negative of the arctangent of the line slopes.

(A color version of this figure is available in the online journal.)

The remaining five sources (G 232.6+1.0, VY CMa, the Orion Nebula, Cep A, and G59.7+0.1) trace the Local (Orion) "arm," which appears to be a spur between the Carina–Sagittarius and Perseus arms. The Sun is in or near this spur, and we can trace it between G 59.7+0.1 near the Carina–Sagittarius arm at $\ell = 60°$ and G 232.6+1.0 near the Perseus arm at $\ell = 233°$.

2.2. Pitch Angles

Spiral arm pitch angles can be estimated when two or more sources can be confidently identified as members of a single arm. The pitch angle, ψ, of an arm segment can be defined by constructing a line segment between sources in the same section of the arm. Next, construct a line tangential to a Galactocentric circle that passes through the midpoint of this segment and determine the angle between these two lines. An ideal log-periodic spiral arm can be defined by the equation

$$\ln(R/R_{\rm ref}) = -(\beta - \beta_{\rm ref}) \tan\psi,$$

where R is the Galactocentric radius at a Galactocentric longitude β (defined as 0 toward the Sun and increasing with Galactic longitude) for an arm with a reference radius $R_{\rm ref}$ at $\beta_{\rm ref}$. In Figure 2, we plot $\log(R/1\ {\rm kpc})$ versus β for the three arms where we can clearly identify two or more HMSFRs. In such a plot, spiral arm sections appear as straight lines. Some of the data deviate from fitted lines by considerably more than the parallax errors, as expected for variations of the locations of star-forming regions within an arm whose width is ~100 pc. Thus we used unweighted straight line fits to estimate spiral arm pitch angles.

The Perseus arm sources (excluding NGC 281) indicate a pitch angle of $16.^\circ5 \pm 3.^\circ1$ between Galactic longitude 112° and 189°. This is in the upper half of pitch angle estimates of 5°–21° for spiral arms in the Galaxy collected by Vallée (1995). The five HMSFRs with parallaxes that trace the Local "arm" indicate a mean pitch angle of $27.^\circ8 \pm 4.^\circ7$. However, the Local arm is probably not a global spiral arm; instead it appears to be a short segment or spur between the Carina–Sagittarius and Perseus arms.

Two sources (S 269 and WB89–437) appear to be part of the Outer arm and formally yield a pitch angle of $2.^\circ3$. This suggests that the Outer arm might have a smaller pitch angle than the Perseus arm. This may be of significance, but with only two sources, more parallaxes are needed before reaching any firm conclusions.

For other spiral arms, we have too few parallaxes to reliably determine pitch angles. The sources that are possible members of the Carina–Sagittarius arm (G 35.2−0.7, G 35.2−1.7 & W 51 IRS 2) would formally give a wide range of pitch angles. However, because one or more sources might be associated with the Local arm, we cannot reliably estimate the pitch angle of the Carina–Sagittarius arm at this time.

3. GALACTIC DYNAMICS

Given measurements of position, parallax, proper motion, and Doppler shift, one has complete three-dimensional location and velocity vectors relative to the Sun. One can then construct a model of the Milky Way and adjust the model parameters to best match the data. We model the Milky Way as a disk rotating with speed $\Theta(R) = \Theta_0 + \frac{d\Theta}{dR}(R - R_0)$, where R_0 is the distance from the Sun to the Galactic center. We started the fitting process by assuming a flat rotation curve (i.e., $\frac{d\Theta}{dR} = 0$). Later, we relaxed this assumption and solved for $\frac{d\Theta}{dR}$, followed by an investigation of other forms of the Galactic rotation curve. Since all measured

Table 2
Galaxy Model Parameter Definitions

Parameter	Definition
R_0	Distance of Sun from GC
Θ_0	Rotation Speed of Galaxy at R_0
$\frac{d\Theta}{dR}$	Derivative of Θ with R: $\Theta(R) = \Theta_0 + \frac{d\Theta}{dR}(R - R_0)$
$U_\odot$	Solar motion toward GC
$V_\odot$	Solar motion in direction of Galactic rotation
$W_\odot$	Solar motion toward NGP
$\overline{U_s}$	Average source peculiar motion toward GC
$\overline{V_s}$	Average source peculiar motion in direction of Galactic rotation
$\overline{W_s}$	Average source peculiar motion toward NGP

Notes. GC is the Galactic center and NGP is the north Galactic pole. The average source peculiar motions ($\overline{U_s}$, $\overline{V_s}$, $\overline{W_s}$) are defined at the location of the source and are rotated with respect to the solar motion ($U_\odot$, $V_\odot$, $W_\odot$) by the Galactocentric longitude, β, of the source (see Figure 8). We solve for the magnitude of each component, but the orientation of the vector for each source depends on location in the Galaxy.

motions are relative to the Sun, we need to remove the peculiar (noncircular) motion of the Sun, which is parameterized by $U_\odot$ toward the Galactic center, $V_\odot$ in the direction of Galactic rotation, and $W_\odot$ toward the north Galactic pole (NGP). Table 2 summarizes these and other parameters.

We adjusted the Galactic parameters so as to best match the data to the spatial-kinematic model in a least-squares sense. For each source, we treated the measured parallax (π_s), two components of proper motion (μ_x, μ_y), and the heliocentric velocity ($v_{\rm Helio}$) as data. The observed source coordinates are known to extremely high accuracy and were treated as independent variables. The model is a smoothly rotating galaxy given by the parameters listed in Table 2. Specifically, the model parallax is calculated from a kinematic distance, based on the observed Doppler shift. The three-dimensions of motion relative to the Sun (proper motion and heliocentric Doppler shift) are calculated from the source location, taking into account the size and rotation curve of the galaxy model, and the solar and source peculiar motions. We adopt the *Hipparcos* determination of solar motion (Dehnen & Binney 1998) as definitive and generally did not vary these parameters. However, in one least-squares fit, we solved for these parameters for illustrative purposes in order to compare solar motion results from *Hipparcos* stars and our HMSFRs.

Our choice of weights for the data in the least-squares fitting process requires some comment. While the heliocentric velocity of any maser spot can be measured with very high accuracy, it may not exactly reflect the motion of the HMSFR. The internal motions of methanol masers are generally small and cause uncertainty of $\approx$3 km s^{-1} (Moscadelli et al. 2002), whereas H_2O masers can be associated with fast outflow and, if not accurately modeled, can lead to larger uncertainty in the motion of the exciting star. In addition, the virial motion of an individual massive star (associated with the masers) with respect to the entire HMSFR is likely to be $\approx$7 km s^{-1} per coordinate (e.g., for a region of mass of $\sim 3 \times 10^4 M_\odot$ and radius of $\sim$1 pc). Therefore, we allow for a deviation of the measured motion from the center of mass of its associated HMSFR by adding an uncertainty of $\sigma_{\rm Vir} = 7$ km s^{-1} in quadrature with the internal motion estimates (between 3 and 5 km s^{-1}). Specifically, the variance weights for the $v_{\rm LSR}$ data, $w(v_{\rm LSR})$, are calculated from $w(v_{\rm LSR}) = 1/(\sigma^2_{v_{\rm LSR}} + \sigma^2_{\rm Vir})$.

Since the parallax data is compared to a kinematic model, we considered both the parallax measurement uncertainty and a modeling uncertainty for the kinematic distance, σ_{kd}, owing to the total uncertainty in the heliocentric velocity of the associated HMSFR. These two components were added in quadrature when calculating the weights: $w(\pi_s) = 1/(\sigma^2_\pi + \sigma^2_{kd}/d_s^4)$, where $d_s = 1/\pi_s$. Similarly, the proper motion weights allowed for both measurement uncertainties and the possible deviation of the measured maser motions from the center of mass of the HMSFR. The latter term was set by the uncertainty in the heliocentric velocity divided by the distance. Thus, for either proper motion component, $w(\mu) = 1/\left(\sigma^2_\mu + \sigma^2_{\rm Vir}/d_s^2\right)$.

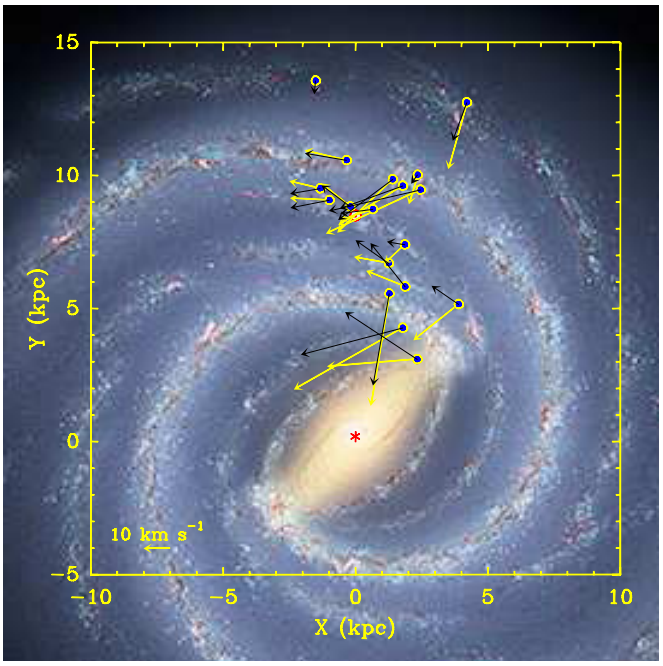

Figure 3. Peculiar motion vectors of HMSFRs (superposed on an artist conception) projected on the Galactic plane after transforming to a reference frame rotating with the Galaxy. A 10 km s^{-1} motion scale is in the lower left. The Galaxy is viewed from the north Galactic pole and rotates clockwise. The light (yellow) arrows are for IAU standard values of $R_0 = 8.5$ kpc and $\Theta_0 = 220$ km s^{-1} and a flat rotation curve, whereas black arrows are for $\Theta_0 = 254$ km s^{-1}. This demonstrates that the qualitative result that HMSFRs orbit the Galaxy slower than the Galaxy rotates is not sensitive to the value of Θ_0.
(A color version of this figure is available in the online journal.)

3.1. Galactic Three-Dimensional Motions

We first used all 18 sources listed in Table 1 and solved only for the fundamental Galactic parameters, yielding $R_0 = 8.2$ kpc and $\Theta_0 = 265$ km s^{-1} for a flat rotation curve ($\frac{d\Theta}{dR} = 0$; see Fit 1 in Table 3). The χ^2 value of 263 for 70 degrees of freedom was quite large, and the post-fit residuals showed clear systematic deviations, indicating a deficiency in this two-parameter model for Galactic dynamics.

Figure 3 shows the peculiar motions of the HMSFRs in the Galactic plane by transforming to a reference frame that rotates with the Galaxy. Peculiar motions relative to two Galactic rotation models are shown, one for $\Theta_0 = 220$ km s^{-1} (the IAU recommended value) and the other for $\Theta_0 = 254$ km s^{-1} (our best fit value from Section 3.2 below). Both transformations assume $R_0 = 8.5$ kpc, a flat rotation curve, and the *Hipparcos* solar motion of Dehnen & Binney (1998). (The equations used for the transformation are documented in the Appendix.) Sizeable systematic motions are clearly evident—almost all

Table 3
Least-squares Fitting Results

Fit	R_0 (kpc)	Θ_0 (km s^{-1})	$\frac{d\Theta}{dR}$ (km s^{-1} kpc^{-1})	$\overline{U_s}$ (km s^{-1})	$\overline{V_s}$ (km s^{-1})	$\overline{W_s}$ (km s^{-1})	χ^2	DF	Θ_0/R_0 (km s^{-1} kpc^{-1})
1	8.24 ± 0.55	265 ± 26	0.0	0.0	0.0	0.0	263.3	70	32.4 ± 1.3
2	8.50 ± 0.44	264 ± 19	0.0	3.9 ± 2.5	-15.9 ± 2.1	-3.1 ± 2.5	111.5	67	31.1 ± 1.1
3	8.40 ± 0.36	254 ± 16	0.0	2.3 ± 2.1	-14.7 ± 1.8	-3.0 ± 2.2	66.7	59	30.3 ± 0.9
4	9.04 ± 0.44	287 ± 19	2.3 ± 0.9	1.9 ± 2.0	-15.5 ± 1.7	-3.0 ± 2.1	59.0	58	31.1 ± 0.9
5	8.73 ± 0.37	272 ± 15	Clemens-10	1.7 ± 1.9	-12.2 ± 1.7	-3.1 ± 1.9	52.9	59	31.0 ± 0.8
6	7.88 ± 0.30	230 ± 12	Clemens-8.5	2.7 ± 2.2	-12.4 ± 1.9	-3.1 ± 2.3	71.2	59	29.6 ± 1.0
7	8.79 ± 0.33	275 ± 13	Brand–Blitz	1.9 ± 2.0	-18.9 ± 1.8	-3.0 ± 2.1	59.0	59	31.0 ± 0.9

Notes. Fits 1 and 2 used all 18 sources in Table 1 and have high χ^2 values, owing to two outliers: NGC 7538 and G 23.6−0.1. Fit 3 excludes the two outliers and provides our basic result, under the assumption of a flat rotation curve. Fits 4–7 explore the effects of nonflat rotation curves. "DF" is the degrees of freedom for the fit (i.e., number of data equations minus number of parameters). ($\overline{U_s}$, $\overline{V_s}$, $\overline{W_s}$) are average peculiar motions common to all sources (see Table 6 and Figure 8), assuming the *Hipparcos* solar motion of Dehnen & Binney (1998) (see discussion in Section 3.1). All Θ_0/R_0 estimates were obtained by holding $R_0 = 8.50$ kpc and solving for Θ_0. "Clemens-10" and "Clemens-8.5" refer to the Clemens (1985) rotation curves for (R_0 (kpc),Θ_0 (km s^{-1})) = (10, 250) and (8.5, 220), respectively; "Brand–Blitz" refers to the Brand & Blitz (1993) rotation curve. Both the Clemens and Brand–Blitz rotation curves were scaled to the fitted values of R_0 and Θ_0.

sources have a significant component of peculiar motion *counter* to Galactic rotation. On average these star-forming regions orbit the Galaxy ≈15 km s^{-1} slower than the Galaxy spins. As is evident from the two sets of peculiar motions, this conclusion is insensitive to the values adopted for Θ_0. Similarly, adopting a more complex rotation curve, e.g., the Clemens (1985) curve, would not change the qualitative nature of the residuals. *HMSFRs appear to orbit the Galaxy slower than for circular orbits.* This might be explained by star formation triggered by the encounter of molecular gas with a shock front associated with a trailing spiral arm and may help explain the 17 km s^{-1} dispersion seen in H I data by Brand & Blitz (1993).

For the distribution of sources in our sample, the solar motion parameters $U_\odot$ and $V_\odot$ can partially mimic the average source peculiar motions. We believe the solar motion parameters determined from *Hipparcos* data by Dehnen & Binney (1998) are well determined, and they have been independently confirmed by Méndez et al. (1999), based on the Southern Proper-Motion program data. However, it is instructive to solve for the solar motion parameters with the parallax and proper motion data. Doing so we find an acceptable fit with $R_0 = 8.4$ kpc, $\Theta_0 = 242$ km s^{-1}, $U_\odot = 9$ km s^{-1}, $V_\odot = 20$ km s^{-1}, and $W_\odot = 10$ km s^{-1}. (The χ^2 value for this fit was 67.2 for 59 degrees of freedom, which is somewhat worse than the value of 65.7 found in Section 3.2, where we adopt the *Hipparcos* solar motion parameters and solved instead for average source peculiar motion components.)

In Figure 4, we reproduce the *Hipparcos* solar motion data from Figure 4 of Dehnen & Binney (1998). Their data were binned by stellar colors, plotted against stellar dispersion and the solar motion components estimated as minus the average velocity of all stars in each bin. We have also plotted our estimates of the solar motion, plotted at near-zero "stellar dispersion" appropriate for newly formed stars. Also included in the bottom panel is the value of $W_\odot$ determined from the proper motion of Sgr A* by Reid & Brunthaler (2004), assuming that the supermassive black hole is stationary at the Galactic center. These values for $U_\odot$ and $W_\odot$ are in good agreement with the *Hipparcos* results.

The *Hipparcos* data used to determine $V_\odot$ (the solar motion component in the direction of Galactic rotation) clearly show the well known "asymmetric drift," which when extrapolated to zero dispersion should define the LSR. Our value of $V_\odot =$

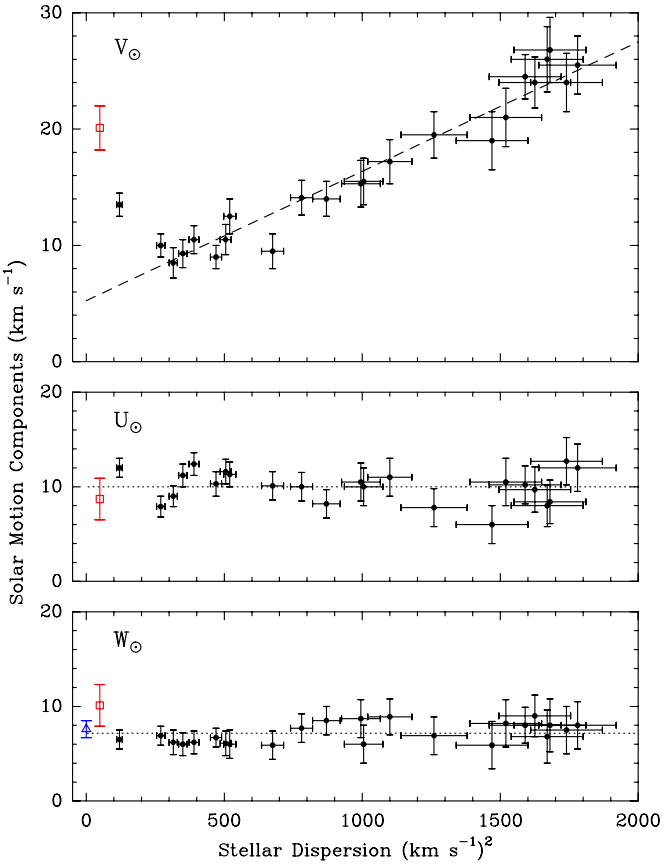

Figure 4. Solar motion components determined from *Hipparcos* stars (i.e., the reflex of the average motion of stars) vs. stellar velocity dispersion after Dehnen & Binney (1998). Top Panel: $V_\odot$ is the Solar Motion in the direction of Galactic rotation (i.e., toward $\ell = 90°$). The "asymmetric drift" is shown with the dashed line. Middle Panel: $U_\odot$ is the Solar Motion toward the Galactic center. Bottom Panel: $W_\odot$ is toward the north Galactic pole. Also plotted at 50 (km s^{-1})^2 dispersion with open red squares are solar motion parameters obtained from the parallax and proper motions of star forming regions, and at zero dispersion with an open triangle is the $W_\odot$ component inferred from the proper motion of Sgr A* by Reid & Brunthaler (2004). Note the good agreement of the $U_\odot$ and $W_\odot$ components between *Hipparcos* and this study. The large deviation of the $V_\odot$ component from the asymmetric drift from this study is not indicative of large $V_\odot$ value, but points to a significant deviation from circular orbits for very young stars.

(A color version of this figure is available in the online journal.)

20 km s^{-1}, based on HMSFR parallaxes and proper motions, is far above the asymmetric drift line, indicating that the HMSFRs as a group are orbiting the Galaxy slower than for circular orbits. Note that the youngest stars in the *Hipparcos* data, plotted at a dispersion of $\approx$120 (km s^{-1})^2, show a similar, but not as great a departure from the asymmetric drift line. Evidence that young stars lag the LSR orbit has also been found by Zabolotskikh et al. (2002).

Finally, we note that we find no evidence for a global motion of the LSR (i.e., disagreement with the *Hipparcos* solar motion) in the direction of the Galactic center or out of the plane of the Galaxy larger than 6 km s^{-1} (2σ). This is contrary to the conclusions of Kerr (1962) and Blitz & Spergel (1991a), based on an analysis of H I data, that the LSR is moving away from the Galactic center at a speed of > 10 km s^{-1}.

3.2. Fundamental Galactic Parameters

Since, as shown in Section 3.1, HMSFRs are orbiting the Galaxy slower than for circular orbits, we must allow for such effects when modeling the Galaxy. In order to determine the fundamental parameters R_0 and Θ_0, we solved for three additional parameters, allowing for an average peculiar motion for all sources with components $\overline{U_s}$ toward the Galactic center (as seen by the source), $\overline{V_s}$ in the local direction of Galactic rotation, and $\overline{W_s}$ toward the north Galactic pole. This solution, listed as Fit 2 in Table 3, yields $R_0 = 8.5$ kpc and $\Theta_0 = 264$ km s^{-1} and peculiar motion components of $\overline{U_s} = 4$ km s^{-1}, $\overline{V_s} = -16$ km s^{-1} and $\overline{W_s} = -3$ km s^{-1}. The residuals show greatly reduced systematic deviations, and the χ^2 value improved significantly to 112 for 67 degrees of freedom, compared to the solution without the average peculiar motions (Fit 1 in Table 3).

Two sources from the sample, NGC 7538 and G 23.6−0.1, displayed post-fit residuals significantly greater ($> 3\sigma$) than the others. Removing these sources, we arrive at our "basic sample" of 16 HMSFRs. We repeated the fitting and found $R_0 = 8.40 \pm 0.36$ kpc, $\Theta_0 = 254 \pm 16$ km s^{-1}, $\overline{U_s} = 2.3 \pm 2.1$ km s^{-1}, $\overline{V_s} = -14.7 \pm 1.8$ km s^{-1}, and $\overline{W_s} = -3.0 \pm 2.1$ km s^{-1} (see Fit 3 in Table 3). The χ^2 value for this sample was considerably improved: 65.7 for 59 degrees of freedom. The near-zero average motion out of the plane of the Galaxy ($\overline{W_s}$) is as expected for massive star-forming regions. The residual motions in the plane of the Galaxy are shown in Figure 5. Most of the star-forming regions have residual velocities consistent with measurement error combined with expected virial motions within HMSFRs of $\sim$7 km s^{-1} per coordinate. The most distant sources at low declination (and low Galactic longitude) have larger residual velocities owing to greater parallax and proper motion measurement uncertainty and the scaling of proper motions to linear speeds by multiplying by distance.

We feel that this solution provides the best estimates of the parameters for the current data set, under the assumption of a flat rotation curve. In Section 3.3, we show that the estimate of R_0 is somewhat sensitive to the nature of the rotation curve of the Galaxy, leading to a systematic source of uncertainty for R_0 of approximately ± 0.5 kpc. Combining the statistical and systematic uncertainties in quadrature, we find $R_0 = 8.4 \pm 0.6$ kpc.

The correlation coefficient between R_0 and Θ_0 was 0.87, while all others were small. This is expected, since kinematic model distances increase with R_0 and inversely with Θ_0. Thus, the ratio Θ_0/R_0, which is the angular rotation rate of the LSR, is determined to much better accuracy than either parameter separately. Holding $R_0 = 8.50$ kpc (the IAU recommended value), we find $\Theta_0 = 257.9 \pm 7.7$ km s^{-1} or $\Theta_0/R_0 = 30.3 \pm 0.9$ km s^{-1} kpc^{-1}. There is only a slight dependence of Θ_0/R_0 on the value adopted for R_0. For example, setting $R_0 = 8.00$ kpc, we obtain $\Theta_0/R_0 = 30.0 \pm 0.9$ km s^{-1} kpc^{-1}. See Section 6 for a discussion of the significance of this result.

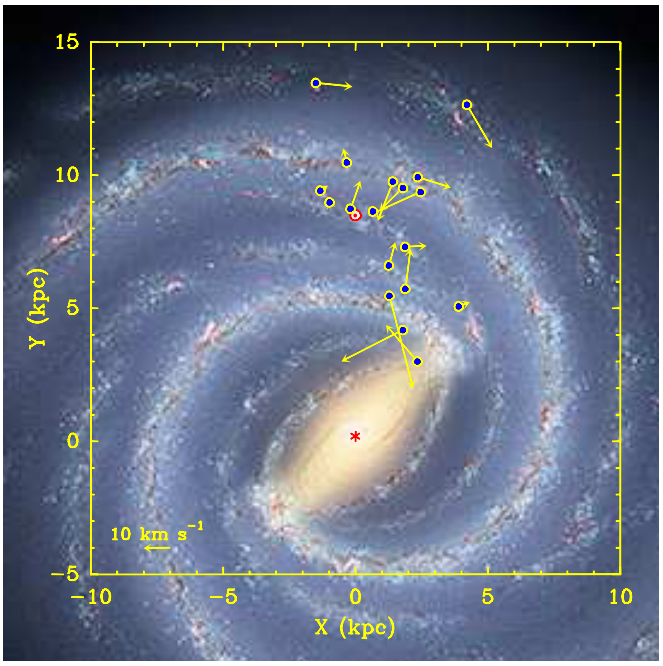

Figure 5. Peculiar motion vectors of high mass star-forming regions (superposed on an artist conception) after transforming to a reference frame rotating with the Galaxy, using best-fit values of $R_0 = 8.4$ kpc and $\Theta_0 = 254$ km s^{-1} and removing an average motion of 15 km s^{-1} counter to Galactic rotation and 2 km s^{-1} toward the Galactic center. A 10 km s^{-1} motion scale is in the lower left. The Galaxy is viewed from the north Galactic pole and rotates clockwise.
(A color version of this figure is available in the online journal.)

As shown in Section 3.3, while estimates of Θ_0 change by ± 20 km s^{-1} among the fits using different rotation curves, this variation can be accounted for mostly through the correlation with R_0, and, therefore, the least-squares fitting process incorporates this correlation in the formal uncertainty estimate. Thus, we conclude that the formal uncertainty of ± 16 km s^{-1} for Θ_0 is reasonable (provided that R_0 is within 0.5 kpc of 8.4 kpc). When R_0 is ultimately measured with much higher accuracy, Θ_0 would be even better determined from the well determined ratio of Θ_0/R_0.

We also considered the possibility that a large positive value for $\overline{U_s}$ (toward the Galactic center), as could be expected from spiral density wave theory, might inflate the estimate of Θ_0. Holding $\overline{U_s} = 17$ km s^{-1} (15 km s^{-1} greater than our best fit) did not significantly reduce the estimate of Θ_0, but did dramatically increase the χ^2 to 200.1. Thus, we exclude a large $\overline{U_s}$ value and that it could contribute to significant uncertainty in Θ_0.

3.3. Rotation Curves

We have until now assumed that the rotation curve of the Galaxy is flat (i.e., $\Theta(R) = \Theta_0$). In order to investigate deviations from a flat rotation curve, we used the basic sample

of 16 sources and added the parameter $\frac{d\Theta}{dR}$ to the model. A least-squares fit yielded $\frac{d\Theta}{dR} = 2.3 \pm 0.9$ km s^{-1} kpc^{-1}, with an improved χ^2 compared to the flat rotation curve fit (see Fit 4 in Table 3), but with an increased correlation coefficient between R_0 and Θ_0 of 0.90. We tested how sensitive $\frac{d\Theta}{dR}$ was to the two outer Galaxy sources by dropping S 269 and WB 89-437 from the sample and refitting. This yielded $\frac{d\Theta}{dR} = 1.9 \pm 1.2$ km s^{-1} kpc^{-1} and indicated that these sources do not provide all the leverage for a rising rotation curve. Thus, we find a nearly flat rotation curve between Galactocentric radii of about 4 to 13 kpc, with some evidence for a slight rise with distance from the Galactic center. This supports similar conclusions reached in a number of papers (Fich et al. 1989; Brand & Blitz 1993; Honma & Sofue 1997; Maciel & Lago 2005). For example Fich et al. (1989) find that the rotation curve is nearly flat for $\Theta_0 = 220$ km s^{-1} and that it rises gradually for $\Theta_0 = 250$ km s^{-1}.

We also tested more complex rotation curves by replacing the simple linear form just discussed with the rotation curves of Clemens (1985) and Brand & Blitz (1993). Clemens supplied two curves: one assuming the old IAU constants of $R_0 = 10$ kpc and $\Theta_0 = 250$ km s^{-1} and the other assuming the new constants of $R_0 = 8.5$ kpc and $\Theta_0 = 220$ km s^{-1}. These models have slightly different shapes, with the old model generally having rotational speeds that rise faster with radius than the new model. For either model, we fitted for different values of R_0 (which we used to scale model radii) and Θ_0 (which we used to scale rotation speeds). The fit using the old model, listed as Fit 5 in Table 3, gave $R_0 = 8.7 \pm 0.4$ kpc and $\Theta_0 = 272 \pm 15$ km s^{-1}, with an improved $\chi^2 = 52.9$ for 59 degrees of freedom compared to our solution for a flat rotation curve. The improvement is partly from a better match to the two sources in the Outer arm (S 269 and WB 89-437). Using the new rotation model, gave $R_0 = 7.9 \pm 0.3$ kpc and $\Theta_0 = 230 \pm 12$ km s^{-1}, with a considerably worse $\chi^2 = 71.2$ (see Fit 6 in Table 3). Using the Brand & Blitz (1993) rotation curve, also scaled by the fitted values of R_0 and Θ_0, we obtain Fit 7 in Table 3, with values of $R_0 = 8.8 \pm 0.4$ kpc and $\Theta_0 = 275 \pm 15$ km s^{-1} and a $\chi^2 = 59.0$ for 59 degrees of freedom, intermediate between the χ^2 values for the two Clemens models.

Clearly, there is some sensitivity of the best fit R_0 value to the models, and we adopt a systematic uncertainty in R_0 of ± 0.5 kpc. Note that, as discussed in Section 3.2, the ratio Θ_0/R_0 has much less modeling sensitivity. With the current parallax and proper motion data, we cannot conclusively distinguish among the rotation curves presented. However, with the many more parallaxes and proper motions expected in the next few years from the VLBA and VERA telescopes, we should be able to make considerable progress in refining the rotation curve of the Milky Way.

4. KINEMATIC DISTANCES

Figure 6 compares the locations of the star-forming regions determined by trigonometric parallax and by kinematic distances. The kinematic distances were computed for the IAU standards $R_0 = 8.5$ kpc and $\Theta_0 = 220$ km s^{-1} and the standard definition of LSR. For 13 of 18 regions (11 of 16 in the basic sample), the kinematic distance exceeds the true source distance; in three cases the discrepancy is over a factor of 2. The kinematic distances for (these) star-forming regions tend to over-estimate the source distances.

As shown above, HMSFRs on average orbit the Galaxy $\approx$15 km s^{-1} slower than the circular rotation speed. Taking this into account, a prescription for a "revised" kinematic distance for a HMSFR could be as follows:

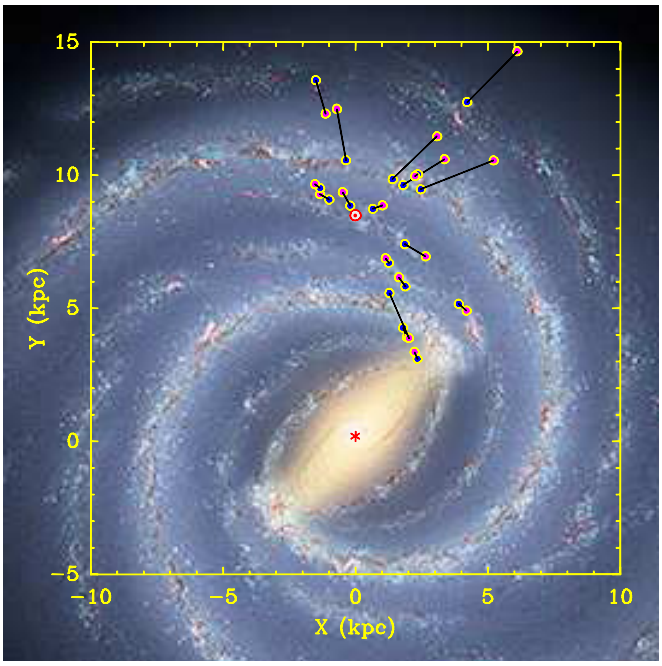

Figure 6. Locations of the star-forming regions determined by trigonometric parallax (dark blue circles) and by kinematic distances (light magenta circles), assuming IAU recommended values of $R_0 = 8.5$ kpc and $\Theta_0 = 220$ km s^{-1} and the standard solar motion to define the LSR.

(A color version of this figure is available in the online journal.)

1. add back the (old) standard solar motion corrections to the LSR velocities, returning them to the heliocentric frame;
2. apply "best values" for the solar motion to calculate a revised "LSR" velocity, $v^r_{\rm LSR}$;
3. subtract -15 km s^{-1} from the velocity component in the direction of Galactic rotation;
4. calculate a kinematic distance using values for the fundamental parameters of the Milky Way, e.g., $R_0 = 8.4$ kpc and $\Theta_0 = 254$ km s^{-1}, that are consistent with astrometric measurements; and
5. when determining the *uncertainty* in the kinematic distance, include a systematic contribution allowing for the possibility of a 7 km s^{-1} uncertainty in $v^r_{\rm LSR}$.

Table 4 shows parallax distances, standard (old) kinematic distances, and revised kinematic distances and uncertainties (using the above prescription) for all 18 HMSFRs listed in Table 1. (We provide the FORTRAN source code used to calculate revised kinematic distances in the online material.) Note that our prescription for the uncertainty in kinematic distances performs reasonably well for our basic sample (excluding the two sources G 23.6−0.1 and NGC 7538 which we earlier noted as outliers). The mean difference between the parallax and kinematic distances is near zero and the differences divided by their uncertainties average to near unity. Now only half (8 of 16) of the sources in the basic sample have kinematic distances that exceed the true source distance. There are no cases for which the discrepancy is a factor of 2, and the estimated uncertainties reasonably account for differences between the parallax and kinematic distances.

While the prescription outlined above results in some improvement in kinematic distances compared to the standard approach, the improvement is not as great as one might at first ex-

Table 4
Parallaxes Versus Kinematic Distances

Source	ℓ (deg)	b (deg)	$v_{\rm LSR}$ km s^{-1}	D_π (kpc)	$D_k^{\rm Std}$ (kpc)	$D_k^{\rm Rev}$ (kpc)
G 23.0−0.4	23.01	−0.41	+81	4.59	4.97	$4.72^{+0.3}_{-0.3}$
G 23.4−0.2	23.44	−0.18	+97	5.88	5.60	$5.29^{+0.3}_{-0.3}$
G 23.6−0.1	23.66	−0.13	+83	3.19	5.04	$4.77^{+0.3}_{-0.3}$
G 35.2−0.7	35.20	−0.74	+28	2.19	2.00	$1.99^{+0.4}_{-0.4}$
G 35.2−1.7	35.20	−1.74	+42	3.27	2.85	$2.76^{+0.4}_{-0.4}$
W 51 IRS 2	49.49	−0.37	+56	5.13	5.52	$5.46^{+1.6}_{-1.6}$
G 59.7+0.1	59.78	+0.06	+27	2.16	3.07	$3.45^{+1.2}_{-1.2}$
Cep A	109.87	+2.11	−10	0.70	1.09	$0.55^{+0.7}_{-0.6}$
NGC 7538	111.54	+0.78	−57	2.65	5.61	$4.64^{+0.7}_{-0.6}$
IRAS 00420	122.02	−7.07	−44	2.13	3.97	$3.18^{+0.6}_{-0.6}$
NGC 281	123.07	−6.27	−31	2.82	2.69	$2.08^{+0.6}_{-0.6}$
W3(OH)	133.95	+1.06	−45	1.95	4.28	$3.42^{+0.7}_{-0.7}$
WB 89-437	135.28	+2.80	−72	5.99	8.68	$6.89^{+1.2}_{-1.0}$
S 252	188.95	+0.89	+11	2.10	4.06	$3.33^{+4.2}_{-2.4}$
S 269	196.45	−1.68	+20	5.29	4.13	$3.35^{+2.0}_{-1.5}$
Orion	209.01	−19.38	+10	0.41	0.99	$0.71^{+0.7}_{-0.6}$
G 232.6+1.0	232.62	+1.00	+23	1.68	1.92	$1.44^{+0.6}_{-0.5}$
VY CMa	239.35	−5.06	18	1.14	1.56	$1.10^{+0.6}_{-0.6}$

Notes. D_π is the measured parallax converted to distance; $D_k^{\rm Std}$ is the kinematic distance based on standard LSR velocities; $D_k^{\rm Rev}$ and $\sigma(D_k)$ is the revised kinematic distance and its uncertainty, calculated for $R_0 = 8.4$ kpc, $\Theta_0 = 254$ km s^{-1}, and $\overline{U_s} = -15$ km s^{-1}, following the prescription outlined in Section 4. All kinematic distances assume a flat rotation curve.

pect. This occurs because the definition of the LSR uses the standard solar motion. While the standard solar motion differs only slightly from the *Hipparcos* solar motion for components toward the Galactic center ($U_\odot$) and the north Galactic pole ($W_\odot$), there is a large discrepancy for the component in the direction of Galactic rotation. The standard value is $V_\odot^{\rm Std} = 15.3$ km s^{-1}, whereas the *Hipparcos* value is $V_\odot^{H} = 5.25$ km s^{-1}. The +10 km s^{-1} "error" in $V_\odot^{\rm Std}$ partially compensates for the 15 km s^{-1} slower Galactic orbits of HMSFRs shown in Section 3.1. (Note that a positive change in the solar motion component $V_\odot$ results in a negative change in a source peculiar motion component $\overline{V_s}$). Even with the improved prescription for kinematic distances, one cannot really hope to discern spiral structure using kinematic distances.

5. GALACTIC COORDINATES

There is excellent agreement between the two independent VLBI measurements of Θ_0/R_0: the measurement based on parallaxes and proper motions of HMSFRs (this paper) and based on the proper motion of Sgr A* (Reid & Brunthaler 2004). This gives us confidence that (1) we can well model the Galaxy with parallax and proper motions of HMSFRs and (2) Sgr A* is indeed a supermassive black hole at the dynamical center of the Milky Way. These findings offer an independent definition of the Galactic plane and Galactic coordinates. Currently, the IAU definition of the Galactic plane is based primarily on the thin distribution of neutral hydrogen 21 cm emission (Blaauw et al. 1960). The Sun is defined to be precisely in the plane and the origin of longitude was set by the centroid of the radio emission of the large, complex source Sgr A. The Sun is now known to be ≈20 pc north of the plane (see Reed 2006 and references therein) and the supermassive black hole, Sgr A*, is offset by a few arcmin from the IAU defined center.

In the future, one could consider redefining Galactic coordinates based, in part, on the proper motion of Sgr A*, which, after correction for the well-determined solar motion component perpendicular to the Galactic plane, gives the orbital plane of the LSR. The zero of longitude would be best defined by the position of Sgr A*. This would place our supermassive black hole at the origin of Galactic coordinates, and one could rotate the reference frame to remove the Sun from its special location precisely in the Galactic plane.

6. DISCUSSION

VLBI now routinely yields parallax measurements with accuracies of ∼10 μas, corresponding to 10% uncertainty at a distance of 10 kpc, and proper motions that are usually accurate to ∼10 μas y^{-1} or better than ∼1 km s^{-1} at similar distances. Target sources include molecular masers associated with star formation and red giant stars, as well as nonthermal continuum emission associated with young T Tau stars and cool dwarfs. Combining the first results of parallaxes for HMSFRs from the VLBA and the Japanese VERA project has allowed us to begin to investigate the spiral structure and kinematics of the Galaxy.

We have accurately located three of the spiral arms of the Milky Way and directly measured a pitch angle of 16° for a portion of the Perseus spiral arm. This pitch angle is similar to those of spiral arms in other galaxies of type Sb to Sc (Kennicutt 1981). Two armed spirals can account for most of the known large H II regions only if the arms wrap twice around the Galaxy; this requires pitch angles of ≈8°. With pitch angles greater than ≈12°, the Galaxy needs to have four arms in order to account for the approximate locations of H II regions (Georgelin & Georgelin 1976; Taylor & Cordes 1993). There has been considerable discussion in the literature concerning the number of spiral arms in the Galaxy (Simonson 1976; Bash 1981; Vallée 1995; Drimmel 2000; Drimmel & Spergel 2001; Benjamin et al. 2005; Nakanishi & Sofue 2006; Steiman-Cameron et al. 2008), with Spitzer GLIMPSE survey results suggesting that only two arms can be traced in the redder, older population of stars (Benjamin 2008). Perhaps, the VLBI and infrared survey results can be reconciled if the Milky Way exhibits a hybrid structure, consisting of two dominant spiral arms, populated by both young and old stars and with pitch angles near 16°, and two weaker arms traced only by young stars.

Our finding that HMSFRs on average orbit the Galaxy ≈15 km s^{-1} slower than expected for circular orbits has implications for star formation and spiral density wave theory. The plot of the *apparent* solar motion in the direction of Galactic rotation ($V_\odot$) versus stellar dispersion (Figure 4) can be interpreted as a time sequence, with stellar age increasing with dispersion. The 15 km s^{-1} slower orbital speed of HMSFRs displays as a positive departure of the apparent solar motion with respect to the asymmetric drift (the fitted trend to the *Hipparcos* data shown in Figure 4), since the Sun *appears* to orbit faster when measured against such stars. One explanation for this finding is that HMSFRs are born in elliptical Galactic orbits, near apocenter, with orbital eccentricity of about 0.06. As young stars continue to orbit the Galaxy, their orbits become more circularized, as evidenced by the lesser departure of the youngest *Hipparcos* bin (mostly late B-type stars) from the asymmetric drift line compared to the HMSFRs. The gradual transfer of angular momentum from gas to stars in the Galaxy proposed by Chakrabarti (2008) may explain this. At a stellar dispersion of ≈300 (km s^{-1})^2, which corresponds to A2- to A5-type stars with colors $B - V = 0.1$ and characteristic main-sequence lifetimes of ∼1 Gy, the stars join the asymmetric

drift. As stars continue to age, their orbits are progressively "randomized" and they (again) become part of a slower orbiting population, which appears as a larger apparent $V_{\odot}$.

Parallaxes measurements alone generally cannot yield R_0 (except for a parallax of Sgr A*). However, since galaxies rotate in a fairly smooth fashion, a kinematic model can be directly compared with distance and relative motion measurements in order to estimate R_0 and Θ_0. In this paper, we have demonstrated that parallax and proper motion measurements for HMSFRs across large portions of the Galaxy can separate estimates of R_0 and Θ_0, although because of the somewhat restricted coverage of the Galaxy currently available, we have a significant correlation between these parameters. Our best estimate of R_0 is 8.4 ± 0.36 ± 0.5 kpc, where the second uncertainty is systematic and comes from our lack of detailed knowledge of the rotation curve of the Galaxy. This estimate is consistent with the "best" R_0 of 8.0 ± 0.5 kpc from a combination of many methods reviewed by Reid (1993). Also, recent *direct* estimates of R_0 from radial velocities and elliptical paths of stars that orbit Sgr A* have converged on values of 8.4 ± 0.4 kpc (Ghez et al. 2008) and 8.33 ± 0.35 (Gillessen et al. 2009). (These estimates assume that Sgr A* is nearly motionless at the Galactic center. Relaxing this assumption decreases the estimates to about 8.0 kpc.) Of course, many other less direct estimates of R_0 can be found in the literature and span a much greater range.

The characteristic rotation speed of the Galaxy (Θ_0) is a crucial parameter not only for Galactic dynamics and kinematic distance determinations, but also for estimating the total mass in dark matter and the history and fate of the Local Group of galaxies (Loeb et al. 2005; Shattow & Loeb 2008). Estimates of the rotation speed of the Galaxy from the recent literature span a very large range between 184 km s^{-1} (Olling & Merrifield 1998) and 272 km s^{-1} (Méndez et al. 1999). Most estimates of Θ_0 are based on analyses of the shear and vorticity of large samples of stars in the (extended) solar neighborhood and thus really measure Oort's A and B parameters. Quoted values of Θ_0 then come by *assuming* a value for R_0 and using the relation $\Theta_0 = R_0(A - B)$. Our result that $\Theta_0 = 254 \pm 16$ km s^{-1} was obtained by fitting for both R_0 and Θ_0 using full three-dimensional locations and motions of sources well beyond the extended solar neighborhood and, thus, does not assume a value for R_0. However, as discussed in Section 3.2, with the present distribution of sources there is considerable correlation between R_0 and Θ_0 parameters, which is reflected in the ±16 km s^{-1} formal uncertainty for Θ_0.

Our estimate of the ratio Θ_0/R_0 of 30.3 ± 0.9 km s^{-1} kpc^{-1} is determined more accurately than either parameter individually and is nearly independent of the value of R_0 over the range of likely values between about 8.0 and 8.5 kpc. This value differs considerably from that determined from the IAU values of $\Theta_0/R_0 = 220$ km s^{-1}/8.5 kpc = 25.9 km s^{-1} kpc^{-1} and differs marginally from the Feast & Whitelock (1997) analysis of *Hipparcos* Cepheids of 27.19 ± 0.87 km s^{-1} kpc^{-1}. Recent studies, using samples of OB-type stars within 3 kpc of the Sun (excluding Gould's Belt stars and based on *Hipparcos* data augmented with photometrically determined distances), arrive at $A-B$ between 30 km s^{-1} kpc^{-1} (Uemura et al. 2000) and 32 km s^{-1} kpc^{-1} (Miyamoto & Zhu 1998; Elias et al. 2006), with uncertainties of about ±1.5 km s^{-1}.

Our value for Θ_0/R_0 is in excellent agreement with that determined directly from the *apparent* proper motion of Sgr A* (the supermassive black hole at the Galactic center) of 6.379 ± 0.024 mas yr^{-1} (Reid & Brunthaler 2004). One expects a supermassive black hole to be stationary at the dynamical center of the Galaxy to better than ∼1 km s^{-1} (Chatterjee et al. 2002; Dorband et al. 2003; Reid & Brunthaler 2004). Hence, Sgr A*'s *apparent* motion should be dominated by the effects of the Galactic orbit of the Sun. After correcting for the solar motion of 5.25 km s^{-1} in the direction of Galactic rotation (Dehnen & Binney 1998), Sgr A*'s apparent motion yields a global estimate of $\Theta_0/R_0 = 29.45 \pm 0.15$ km s^{-1} kpc^{-1}. Thus, there is excellent agreement between this and our global and direct method for measuring Θ_0/R_0.

Coupling the Sgr A* motion result of $\Theta_0/R_0 = 29.45 \pm 0.15$ km s^{-1} kpc^{-1} with estimates of R_0 from stellar orbits in the Galactic center (Ghez et al. 2008; Gillessen et al. 2009) of 8.4 ± 0.4 kpc yields $\Theta_0 = 247 \pm 12$ km s^{-1}. This result is also a direct and global measurement of Θ_0 and is independent of our result from parallaxes and proper motions of star-forming regions. Combining the Galactic center and star-forming region estimates gives $\Theta_0 = 250 \pm 10$ km s^{-1}.

It seems clear that Θ_0 is near the upper end of the range of estimates in the literature. We note that both the Galactic center stellar orbit and the star-forming region parallax results assume the *Hipparcos* solar motion of 5.25 km s^{-1} in the direction of Galactic rotation. Only if the interpretation of the asymmetric drift is incorrect or if the entire solar neighborhood orbits the Galactic center ∼30 km s^{-1} slower than the Galaxy spins could Θ_0 be equal to the IAU recommended value of 220 km s^{-1}.

We have determined the rotation speed of the Milky Way at the radius of the Sun to be ≈250 km s^{-1} and the rotation curve to be nearly flat or slightly rising with distance from the Galactic center. These values are nearly identical to those of the Andromeda galaxy (M31) as shown in Figure 7. The rotation curve of Andromeda, determined from H I emission by Carignan et al. (2006) based on interferometric observations of Unwin (1983), indicates a speed of 251 km s^{-1} at a radius of 8 kpc, a slightly rising curve out to about 15 kpc, and a

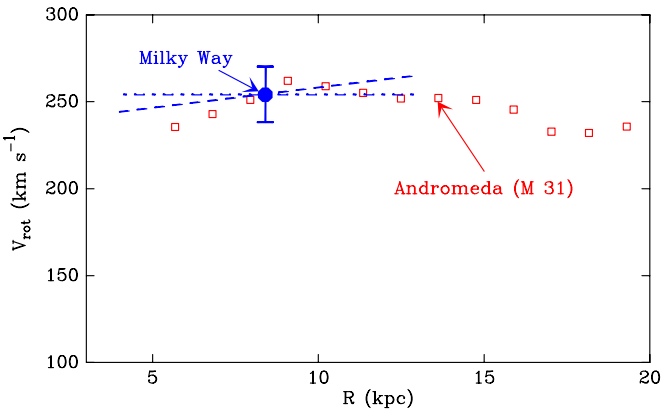

Figure 7. Rotation speed vs. radius for the Andromeda galaxy and the Milky Way. The red squares are based on H I observations of Andromeda tabulated by Carignan et al. (2006). The blue filled circle is our best estimate of $\Theta_0 = 254 \pm 16$ km s^{-1} at $R_0 = 8.4$ kpc for the Milky Way, derived from the parallax and proper motions of HMSFRs. The blue dot-dashed line is for a flat rotation curve, and the blue dashed line corresponds to a slightly rising rotation curve of 2.3 km s^{-1} kpc^{-1}(see Section 3.3). These lines are plotted over the range of Galactocentric radii sampled by the parallax and proper motion results. Note that these two galaxies have nearly identical rotation speeds over this range.

(A color version of this figure is available in the online journal.)

Table 5
Galactic and Solar Parameters and Nominal Values

Parameter	Value	Definition
R_0	8.5 kpc	Distance to the GC (IAU value)
Θ_0	220 km s^{-1}	Rotation speed of LSR (IAU value)
Θ_s	220 km s^{-1}	Rotation speed of Galaxy at source
$U_\odot^{\rm Std}$	10.3 km s^{-1}	Standard Solar Motion toward GC
$V_\odot^{\rm Std}$	15.3 km s^{-1}	Standard Solar Motion toward $\ell = 90^\circ$
$W_\odot^{\rm Std}$	7.7 km s^{-1}	Standard Solar Motion toward NGP
$U_\odot^{H}$	10.0 km s^{-1}	*Hipparcos* Solar Motion toward GC
$V_\odot^{H}$	5.2 km s^{-1}	*Hipparcos* Solar Motion toward $\ell = 90^\circ$
$W_\odot^{H}$	7.2 km s^{-1}	*Hipparcos* Solar Motion toward NGP

Notes. GC: the Galactic center; LSR: local standard of rest; NGP: north Galactic pole. The standard solar motion must be used to convert from $v_{\rm LSR}$ to $v_{\rm Helio}$, since (hopefully) all observatories have used this definition. The values given above come from an assumed solar motion of 20 km s^{-1} toward R.A. (1900) = 18^h and Decl. (1900)-30° precessed to J2000.0. *Hipparcos* solar motion values are from Dehnen & Binney (1998).

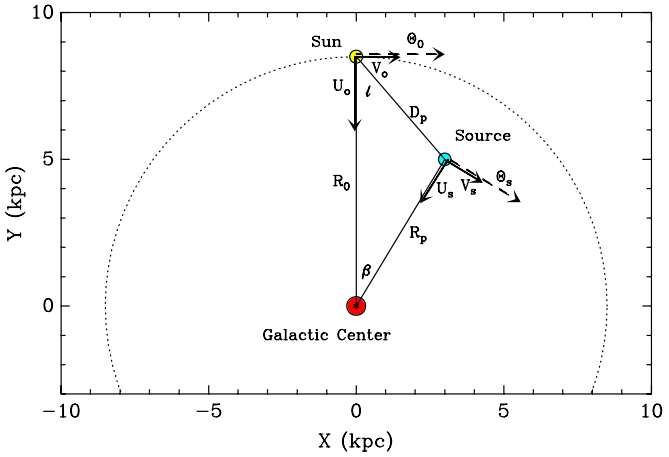

Figure 8. Schematic depiction of source and Galactic parameters.
(A color version of this figure is available in the online journal.)

Table 6
Source Parameter Definitions

Parameter	Definition
ℓ	Galactic longitude
D	Distance from Sun ($1/\pi_s$)
D_p	Distance from Sun projected in plane
R_p	Distance from GC projected in plane
$v_{\rm LSR}$	LSR radial velocity
$v_{\rm Helio}$	Heliocentric radial velocity
μ_α	Proper motion in R.A. ($\mu_\alpha = \mu_x/\cos\delta$)
μ_δ	Proper motion in Decl. ($\mu_\delta = \mu_y$)
β	Angle: Sun–GC–source
U_s	Peculiar motion locally toward GC
V_s	Peculiar motion locally in direction of Galactic rotation
W_s	Peculiar motion toward NGP

Note. GC: the Galactic center; LSR: local standard of rest; NGP: north Galactic pole.

slow dropoff to about 225 km s^{-1} beyond 20 kpc. The most straightforward interpretation of the similarities of the rotation curves for the Milky Way and Andromeda is that these two galaxies are nearly equal in size and mass.

Finally, we note that Reid & Brunthaler (2004) placed a strong upper limit of -0.4 ± 0.9 km s^{-1} for the component of peculiar motion of Sgr A* *perpendicular* to the plane of the Galaxy. However, the determination of the component in the direction of Galactic rotation was considerably less accurate: 18 ± 7 km s^{-1}, as one must remove the uncertain effects of the solar orbit. Reid and Brunthaler did this by removing 27.19 ± 0.87 km s^{-1} kpc^{-1}, based on *Hipparcos* measurements of Oort's constants ($A-B$) by Feast & Whitelock (1997), from the observed motion of Sgr A* in the Galactic plane of 29.45 km s^{-1} kpc^{-1}. This method assumes that $\Theta_0/R_0 = A - B$ and that estimates of the shear and vorticity of nearby stars from *Hipparcos* data indicate the large-scale differential rotation of the Galaxy and are not subject to local irregularities in the solar neighborhood. Since we now have a direct, global estimate of $\Theta_0/R_0 = 30.3 \pm 0.9$ km s^{-1} kpc^{-1}, we find the peculiar motion of Sgr A* in the direction of Galactic rotation to be -7.2 ± 8.5 km s^{-1}, with little sensitivity to R_0 (adopted to be 8.5 kpc here). This adds additional strong evidence that Sgr A* is a supermassive black hole, which is nearly stationary at the dynamical center of the Galaxy.

X.W.Z., B.Z., and Y.X. were supported by the Chinese National Science Foundation, through grants NSF 10673024, 10733030, 10703010 and 10621303, and by the NBPRC (973 Program) under grant 2007CB815403.

APPENDIX

Since we have measured the position, distance, LSR velocity, and proper motion of each source, we know its full three-dimensional location in the Galaxy and full space motion relative to the Sun. Given a model of Galactic rotation, we can then calculate the noncircular (peculiar) velocity of each source. While this calculation is conceptually simple, in practice, there are some subtleties and sign convention issues that can lead to errors, and so here we present the necessary formulae (and FORTRAN source code in the online material).

The required Galactic and solar motion parameters are given in Table 5, and those associated with the source are defined in Table 6. A schematic depiction of these parameters is given in Figure 8. We assume that the Sun is in the Galactic plane and calculate a source's peculiar motion (i.e., with respect to a circular Galactic orbit) as follows.

We convert $v_{\rm LSR}$ to a heliocentric frame, $v_{\rm Helio}$, by adding back the component of the standard solar motion in the line-of-sight direction that had been removed from the observed Doppler shift to calculate $v_{\rm LSR}$. Note that one needs to use the (old) standard solar motion, which defines the LSR frame, and *not* the best values available today. Generally, observatories have adopted a value of 20 km s^{-1} toward $\alpha(1900) = 18^{\rm h}$, $\delta(1900) = +30^{\rm d}$ for the standard solar motion. Precessing these coordinates to the epoch of observation (≈2006) and converting to Galactic Cartesian coordinates yields the ($U_\odot^{\rm Std}$, $V_\odot^{\rm Std}$, $W_\odot^{\rm Std}$) values listed in Table 5. Then,

$$v_{\rm Helio} = v_{\rm LSR} - \left(U_\odot^{\rm Std}\cos\ell + V_\odot^{\rm Std}\sin\ell\right)\cos b - W_\odot^{\rm Std}\sin b.$$

We rotate the motion vector from the equatorial heliocentric frame (μ_α, μ_δ, $v_{\rm Helio}$) to a Galactic heliocentric frame (μ_l, μ_b, $v_{\rm Helio}$). This is a rotation about a radial axis and is defined by the IAU in B1950 coordinates (Blaauw et al. 1960). For coordinates in J2000, Reid & Brunthaler (2004) give the right ascension and declination of the NGP as $\alpha_P = 12^{\rm h}51^{\rm m}26\overset{\rm s}{.}2817$ and $\delta_P = 27^\circ07'42\overset{''}{.}013$, respectively, and the zero of longitude

is the great semicircle originating at the NGP at the position angle $\theta = 122.^{\circ}932$. Galactic latitude can be obtained from

$$\sin b = \sin\delta\cos(90^{\circ} - \delta_P) - \cos\delta\sin(\alpha - \alpha_P - 6^h)\sin(90^{\circ} - \delta_P).$$

A useful angle ϕ can be determined (between 0° and 360°) from

$$\sin\phi = (\cos\delta\sin(\alpha - \alpha_P - 6^h)\cos(90^{\circ} - \delta_P) + \sin\delta\sin(90^{\circ} - \delta_P))/\cos b$$

and

$$\cos\phi = \cos\delta\cos(\alpha - \alpha_P - 6^h)/\cos b,$$

and then Galactic longitude follows from

$$\ell = \phi + (\theta - 90^{\circ}).$$

Proper motion in Galactic coordinates (μ_l, μ_b) can be easily calculated from the motion in equatorial coordinates (μ_α, μ_δ) by differencing (ℓ, b) values for coordinates determined, say, one year apart. This usually requires 64 bit precision in the calculations. Note that μ_l will naturally be defined positive in the direction of increasing Galactic longitude, which is *counter* to Galactic rotation.

Convert the proper motions to linear speeds (by multiplying by distance) via

$$v_\ell = D\mu_l\cos b \quad \text{and} \quad v_b = D\mu_b,$$

where $\mu_l \cos b$ is the actual motion tangent to the sky in the direction of Galactic longitude.

We now convert from spherical to Cartesian Galactic coordinates at the location of the Sun.

$$U_1 = (v_{\rm Helio}\cos b - v_b\sin b)\cos\ell - v_\ell\sin\ell,$$
$$V_1 = (v_{\rm Helio}\cos b - v_b\sin b)\sin\ell + v_\ell\cos\ell,$$
$$W_1 = v_b\cos b + v_{\rm Helio}\sin b.$$

Next, add the full orbital motion of the Sun, using the best values of the solar motion and the circular rotation of the Galaxy at the position of the Sun $(U_\odot^H, V_\odot^H + \Theta_0, W_\odot^H)$,

$$U_2 = U_1 + U_\odot^H,\ V_2 = V_1 + V_\odot^H + \Theta_0,\ W_2 = W_1 + W_\odot^H.$$

The Galactocentric distance to the source projected onto the Galactic plane is given by

$$R_p^2 = R_0^2 + D_p^2 - 2R_0D_p\cos\ell,$$

where $D_p = D\cos b$. The angle β between the Sun and the source as viewed from the Galactic center can be determined in all cases (i.e., from 0° to 360°) from

$$\sin\beta = \frac{D_p}{R_p}\sin\ell \quad \text{and} \quad \cos\beta = \frac{R_0 - D_p\cos\ell}{R_p},$$

Rotate the vector (U_2, V_2, W_2) through the angle β in the plane of the Galaxy and remove circular Galactic rotation at the location of the source to yield (U_s, V_s, W_s),

$$U_s = U_2\cos\beta - V_2\sin\beta,$$
$$V_s = V_2\cos\beta + U_2\sin\beta - \Theta_s,$$
$$W_s = W_2.$$

The vector (U_s, V_s, W_s) gives the noncircular (peculiar) motion of the source in a Cartesian Galactocentric frame, where U_s is radially inward toward the Galactic center (as viewed by the source), V_s is in the local direction of Galactic rotation and W_s is toward the north Galactic pole.

REFERENCES

Bartkiewicz, A., Brunthaler, A., Szymczak, M., van Langevelde, H. J., & Reid, M. J. 2008, A&A, 490, 787
Bash, F. N. 1981, ApJ, 250, 551
Benjamin, R. A. 2008, in ASP Conf. Ser. 387, Massive Star Formation: Observations Confront Theory, ed. eH. Beuther, H. Linz, & Th. Henning (San Francisco, CA: ASP), 375
Benjamin, R. A., et al. 2005, ApJ, 630, L149
Blaauw, A., Gum, C. S., Pawsay, J. L., & Westerhout, G. 1960, MNRAS, 121, 123
Blitz, L., & Spergel, D. N. 1991a, ApJ, 370, 205
Blitz, L., & Spergel, D. N. 1991b, ApJ, 379, 631
Brand, J., & Blitz, L. 1993, A&A, 275, 67
Brunthaler, A., Reid, M. J., Menten, K. M., Zheng, X. W., Moscadelli, L., & Xu, Y. 2009, ApJ, 693, 424 (Paper V)
Burton, W. B., & Bania, T. M. 1974, A&A, 33, 425
Carignan, C., Chemin, L., Huchtmeier, W. K., & Lockman, F. J. 2006, ApJ, 641, L109
Chakrabarti, S. 2008, arXiv:0812.0821
Chatterjee, P., Hernquist, L., & Loeb, A. 2002, ApJ, 572, 371
Choi, Y. K., et al. 2008, PASJ, 60, 1007
Clemens, D. P. 1985, ApJ, 295, 422
Cohen, R. S., Cong, H., Dame, T. M., & Thaddeus, P. 1980, ApJ, 239, L53
Dame, T. M., & Thaddeus, P. 2008, ApJ, 683, L143
Dehnen, W., & Binney, J. J. 1998, MNRAS, 298, 387
Dorband, E. N., Hemsendorf, M., & Merritt, D. 2003, J. Comput. Phys., 185, 484
Drimmel, R. 2000, A&A, 358, L13
Drimmel, R., & Spergel, D. N. 2001, ApJ, 556, 181
Elias, F., Alfaro, E. J., & Cabrera-Caño, J. 2006, AJ, 132, 1052
Feast, M., & Whitelock, P. 1997, MNRAS, 291, 683
Fich, M., Blitz, L., & Stark, A. A. 1989, ApJ, 342, 272
Georgelin, Y. M., & Georgelin, Y. P. 1976, A&A, 49, 57
Ghez, A. M., et al. 2008, ApJ, 689, 1044
Gillessen, S., Eisenhauer, F., Trippe, S., Alexander, T., Genzel, R., Martins, F., & Ott, T. 2009, ApJ, 692, 1075
Gómez, G. C. 2006, AJ, 132, 2376
Hachisuka, K., Brunthaler, A., Menten, K. M., Reid, M. J., Hagiwara, Y., & Mochizuki, N. 2009, ApJ, 696, 1981
Hachisuka, K., et al. 2006, ApJ, 645, 337
Hirota, T., et al. 2007, PASJ, 59, 897
Honma, M., & Sofue, Y. 1997, PASJ, 49, 453
Honma, M., et al. 2007, PASJ, 59, 889
Kennicutt, R. C., Jr. 1981, AJ, 86, 1847
Kerr, F. J. 1962, MNRAS, 123, 327
Liszt, H. S., & Burton, W. B. 1981, ApJ, 243, 778
Loeb, A., Reid, M. J., Brunthaler, A., & Falcke, H. 2005, ApJ, 633, 894
Maciel, W. J., & Lago, L. G. 2005, RevMexAA, 41, 383
Méndez, R. A., Platais, I., Girard, T. M., Kozhurina-Platais, V., & van Altena, W. F. 1999, ApJ, 524, L39
Menten, K. M., Reid, M. J., Forbrich, J., & Brunthaler, A. 2007, A&A, 474, 515
Miyamoto, M., & Zhu, Z. 1998, AJ, 115, 1483
Moellenbrock, G. A., Claussen, M. J., & Goss, W. M. 2007, in IAU Symp. 242, Astrophysical Masers and their Environments, ed. J. M. Chapman & W. A. Baan (Dordrecht: Kluwer), 168
Moellenbrock, G. A., Claussen, M. J., & Goss, W. M. 2009, ApJ, 694, 192
Moscadelli, L., Menten, K. M., Walmsley, C. M., & Reid, M. J. 2002, ApJ, 564, 813
Moscadelli, L., Reid, M. J., Menten, K. M., Brunthaler, A., Zheng, X. W., & Xu, Y. 2009, ApJ, 693, 406 (Paper II)
Nakanishi, H., & Sofue, Y. 2006, PASJ, 58, 847
Olling, R. P., & Merrifield, M. R. 1998, MNRAS, 297, 943
Reed, B. C. 2006, J. R. Astron. Soc. Can., 100, 146
Reid, M. J. 1993, ARA&A, 31, 345
Reid, M. J., & Brunthaler, A. 2004, ApJ, 616, 872
Reid, M. J., Menten, K. M., Brunthaler, A., Zheng, X. W., Moscadelli, L., & Xu, Y. 2009, ApJ, 693, 397 (Paper I)
Russeil, D. 2003, A&A, 397, 133
Sato, M., et al. 2008, PASJ, 60, 975
Shattow, G., & Loeb, A. 2008, MNRAS, 392, L21
Simonson, S. C., III 1976, A&A, 46, 261

Steiman-Cameron, T. Y., Wolfire, M., & Hollenbachg, D. 2008, BAAS Meeting, 40, 213
Taylor, J. H., & Cordes, J. M. 1993, ApJ, 411, 674
Uemura, M., Ohashi, H., Hayakawa, T., Ishida, E., Kato, T., & Hirata, R. 2000, PASJ, 52, 143
Unwin, S. C. 1983, MNRAS, 205, 787
Vallée, J. P. 1995, ApJ, 454, 119
Xu, Y., Reid, M. J., Menten, K. M., Brunthaler, A., Zheng, X. W., & Moscadelli, L. 2009, ApJ, 693, 413 (Paper III)
Xu, Y., Reid, M. J., Zheng, W. W., & Menten, K. M. 2006, Science, 311, 54
Zabolotskikh, M. V., Rastorguev, A. S., & Dambis, A. K. 2002, Astron. Lett., 28, 454
Zhang, B., Zheng, X. W., Reid, M. J., Menten, K. M., Xu, Y., Moscadelli, L., & Brunthaler, A. 2009, ApJ, 693, 419 (Paper IV)